Ultrafine Grained Materials IV. *Edited by Y.T. Zhu, T.G. Langdon, Z. Horita, M.J. Zehetbauer, S.L. Semiatin, and T.C. Lowe*. **TMS (The Minerals, Metals & Materials Society), 2006**

INHOMOGENEOUS AND ANISOTROPIC DEFORMATION BEHAVIOR AND STRAIN HARDENING OF ULTRAFINE-GRAINED ALUMINIUM BY ECAP

Stijn Poortmans[1,*], Fouad El Houdaigui[2], Anne-Marie Habraken[2], Bert Verlinden[1]

[1] Katholieke Universiteit Leuven, Dept. Materials Engineering
Kasteelpark Arenberg 44, B-3001 Heverlee, Belgium
[2]Department of Mechanics of materials and structures
University of Liège, Chemin des Chevreuils 1, B-4000 Liège, Belgium

Abstract

Hot-rolled AA1050 commercial pure aluminum was deformed by ECAP (Equal Channel Angular Pressing) at room temperature following route B_C for 8 passes. Mechanical testing at room temperature on both hot-rolled aluminum and aluminum after ECAP consisted of uniaxial tension, axisymmetric compression and shear by torsion. The phenomenological Hill's criterion identified from texture data accounts for the observed tension-compression asymmetry due to ECAP and predicts torsion yielding close to measurements. FE simulations of the compression tests are performed with a Hill model or a Minty micro-macro model and coupled with an isotropic Voce saturation hardening law. These simulations compute the inhomogeneous behavior due to barreling, the observed sample anisotropy and the force-displacement curve. Comparisons of numerical and experiments results provide a first identification of the hardening parameters and the friction coefficient during compression tests.

Keywords: ECAP, Mechanical testing, Yield Surface, Inhomogeneous deformation

Introduction

The strength of metallic materials is improved by grain size reduction, as described by the Hall-Petch relationship, up to a certain grain size where softening occurs [1]. This decrease in grain size can be obtained by ECAP, producing UFG (ultrafine-grained) materials [2, 3]. During ECAP the material is subjected to a large plastic deformation, causing an increase in strength by work hardening and grain refinement. An additional annealing treatment can restore both ductility and work hardening behavior, while stabilizing the microstructure.

In this study, three types of monotonic tests were investigated: axisymmetric compression, uniaxial tension and shear by torsion. The tests were performed at room temperature on hot rolled aluminum, ECAP-deformed and annealed ECAP material. The influence of deformation and annealing on mechanical properties were investigated before [4]. For each type of material, different yielding and strain hardening could be observed depending on the deformation conditions. These data and texture measurements were then used to identify the initial yield surface and the strain hardening describing the expansion of the yield locus.

Experimental Material and Procedures

The material used in this study is CP-AA1050, hot rolled and fully recrystallized, delivered as 23mm thick plates. All ECAP samples have been machined with the extrusion direction (ED) parallel to the former rolling direction (RD). The samples had a diameter of 12mm and a length of 60mm and were ECAP'ed at room temperature following route B_C [5] for 8 passes, using MoS_2 as lubricant. The ECAP die had an intersection angle Φ=90°, with rounding Ψ=0°. Post-ECAP annealing was carried out in a salt bath for 10 minutes at 300°C.

For mechanical testing, the samples were machined such that only the homogeneous zone would be subjected to deformation. For compressive testing samples had a diameter of 6mm and a height of 9mm. For tensile and torsion testing a cylindrical sample geometry was chosen. The test-zone had a diameter of 5mm and a length of 10mm. Stainless steel custom-made extension parts with screw fixation were used for mounting. Compressive and tensile tests were

performed on an Instron 4505 machine with 100kN load cell. For compressive tests no strains higher than 0.8 are accepted because of barreling. The initial strain rates for compression and tension were $1.5 \cdot 10^{-3}$/s and $8 \cdot 10^{-4}$/s respectively. Torsion tests were performed on a gear shifted cold torsion machine with stretching strips. The shear strain rate was $3.8 \cdot 10^{-4}$/s. To minimize the influence of surface defects, all samples were polished.

To determine the initial yield point, the slope of the stress-strain curve during elastic deformation was used to calculate back 0.2% plastic deformation while accounting for slip and elastic deformation in the extension parts and screw fixation of the sample. For the rate of work hardening the Ludwik formula is used [6], with determination of n for ε_{tot}=1–20%. In order to measure sample anisotropy and the inhomogeneity of deformation due to necking, Laser Interferometry was used. This resulted in a point cloud with average point density of 75 points/mm² with an individual spatial resolution of 0.05mm. The cross-sectional sample shape was assumed to be elliptical and the corresponding elliptical description was determined by the use of a least mean square approximation [7].

Results and Discussion

Mechanical testing – The influence of ECAP on the yield stress and strain hardening under uniaxial compression has been investigated previously [4]. From this study it could be concluded that after 8 passes of ECAP route B_C a (near) steady state was achieved, where no strain hardening under compression was observed. During annealing the yield stress decreased with higher temperature and longer annealing time, also inducing a Lüdersstrain, while the work hardening was recovered. The amount of Lüdersstrain decreases with increasing annealing time. Some representative stress-strain curves are shown in fig 1(a).

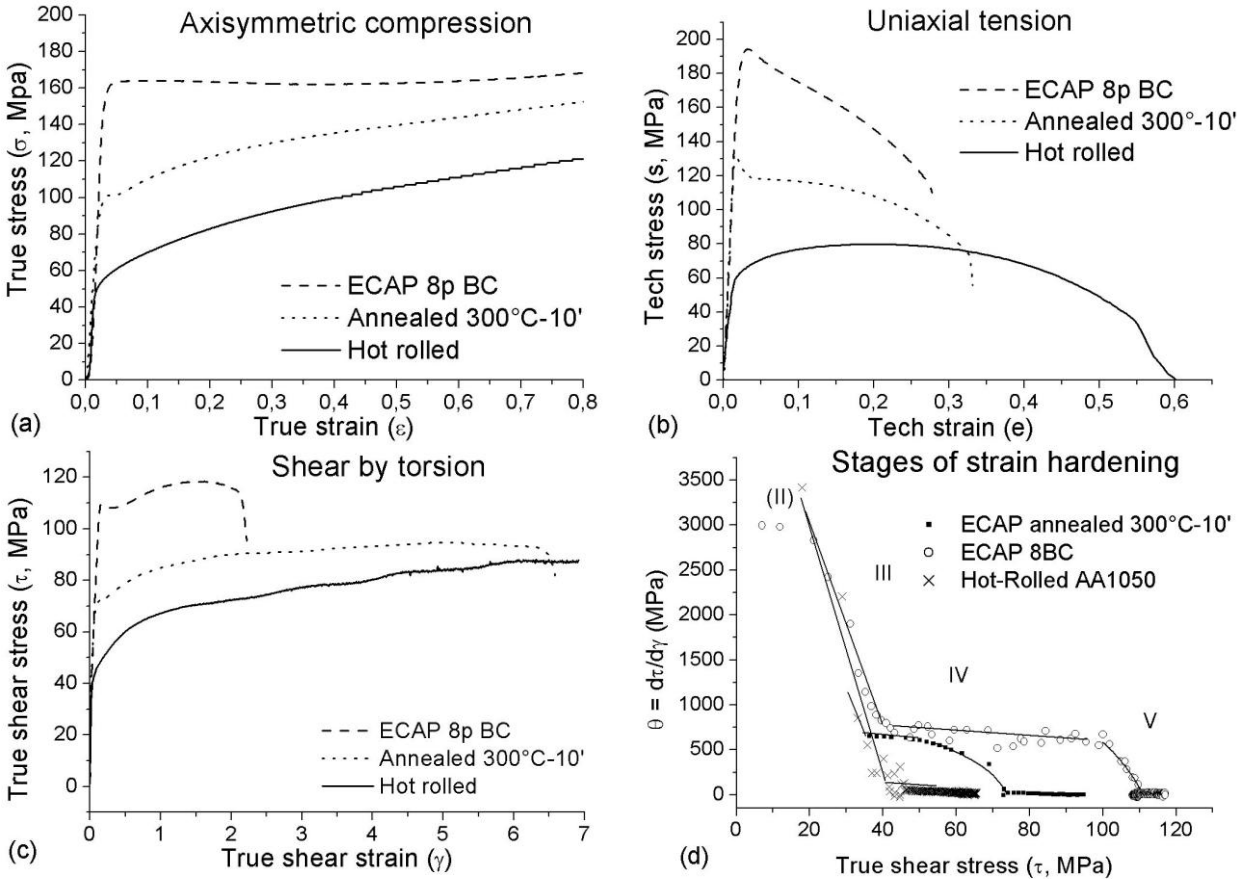

Figure 1 – Results of mechanical testing on hot-rolled AA1050, ECAP 8pass route B_C and annealed ECAP material. (a) Uniaxial compression [σ–ε]; (b) unidirectional tension [s-e]; (c) shear by torsion [τ–γ]; (d) strain hardening stages during torsion.

The values for the initial flow stress and hardening were published before (see also table 1). More information on the interpretation of these updated values can be found in [4].

Table 1 Overview of the mechanical properties under monotonic mechanical testing.

	Tension		Compression		Torsion	
	σ_y (MPa)	n	σ_y (MPa)	n	τ_y (MPa)	n
Hot Rolled	51	0.58	53	0.56	32	0.56
ECAP	186	/	144	/	108	/
Annealed	122	0.56	105	0.57	70	0.56

σ_y : 0.2% offset flow stress.

Following remarks on the values in table 1 must be considered. After ECAP the initial flow stress increases, which is explained by the high amount of dislocations present in the structure. Both the dislocations in the grain interior and the decrease in grain size cause the increase in flow stress. Also the effect of annealing is clear: the grain structure becomes free of dislocations, allowing again a normal strain hardening behavior. In tensile deformation (fig 1(b)) the samples are sensitive to necking, resulting in a smaller uniform deformation. According to May e.a. [10], there is a significant influence of strain rate sensitivity in SPD materials, thus the Hart criterion [11] can be used to determine the onset of necking. As a result of the strain rate sensitivity, the post-uniform elongation is high. Because of this inhomogeneous deformation, the true stress – true strain curve in uniaxial tension, after the onset of necking, can not directly be calculated. Therefore the technical stress and technical strain are shown. The hot-rolled material reveals no difference in yield stress when comparing compression and tensile results, which was to be expected because there are nearly no internal stresses present. Annealing causes the tension-compression anisotropy to decrease, by a combined effect of both release of internal stresses and degradation of the shear structure.

For shear by torsion (fig 1(c)), the τ –γ curves are calculated with the geometrical method (Nadaï formula) [9]. In order to distinguish the different hardening stages, the τ–θ plot is shown in fig 1(d). The hot rolled material exhibits a high ductility, up to an equivalent strain of 4 (τ=7) [9] but its work hardening does not reach stage IV. ECAP material initially has a stage III hardening, succeeded by stage IV. For the annealed ECAP material the initial hardening is nearly regained. The hardening at higher strains is still smaller than for hot rolled material. The torsion results show how the ECAP material has work hardening for γ larger than 1. On the τ–θ curve this is shown as stage IV hardening. Compared with annealed ECAP material, it is obvious how stage III is parallel for all three types, while stage IV is lower and shorter for annealed ECAP material.

Determining the initial Yield Locus – Modeling of the yield loci and strain hardening was focused on the ECAP material. The first goal was to obtain an initial yield surface. Starting from the experimental texture after ECAP, a full-constraints Taylor model was used to calculate the r-ratios, taking into account the crystallographic anisotropy. The r-value as function of theta (angle with axial direction of ECAE sample) according to the Hill model is reminded by equation 1. The known values for theta, 0°, 45° and 90°, allow to compute the 4 independent coefficients for the Hill model, assuming H+G=2 and N=L=M. (F=0.94, G=0.65, H=1.35; N=L=M=2.07).

$$r_\theta = \frac{H + \ 2N - F - G - 4H \ \ \sin^2\theta\cos^2\theta}{F\sin^2\theta + G\cos^2\theta} \tag{1}$$

Also a Taylor-Bisshop-Hill model (THB) was used to calculate the initial yield surface taking into account the crystallographic texture. The section of the yield loci with respect to the crystallographic texture is shown in fig 2(a). A tension $\boldsymbol{\sigma}_y^t$ -compression $\boldsymbol{\sigma}_y^c$ asymmetry can be observed (fig 1) and explained in terms of internal stresses, decreasing during the annealing treatment (and increasing grain size). In the phenomenological model, this is introduced as a backstress, shifting the center of the yield surface. For the ECAP material, this backstress or internal stress is 21MPA, giving a plastic radius of the yield locus, equal to 165MPa.

$$BS = \ \sigma_y^t - \sigma_y^c \ / 2 = \ 186 - 144 \ / 2 = 21MPa \tag{2}$$

$$\sigma_y^{NY} = \ \sigma_y^t + \sigma_y^c \ / 2 = \ 186 + 144 \ / 2 = 165MPa \tag{3}$$

When applying this backstress to the TBH-calculation of the yield locus and comparing with experimental data from the shear in the torsion tests, the use of this backstress gives the best agreement concerning prediction of the flow stress in shear deformation (fig 2(b)). It must be remarked that geometry of the torsion test causes inhomogeneous initial plastic straining.

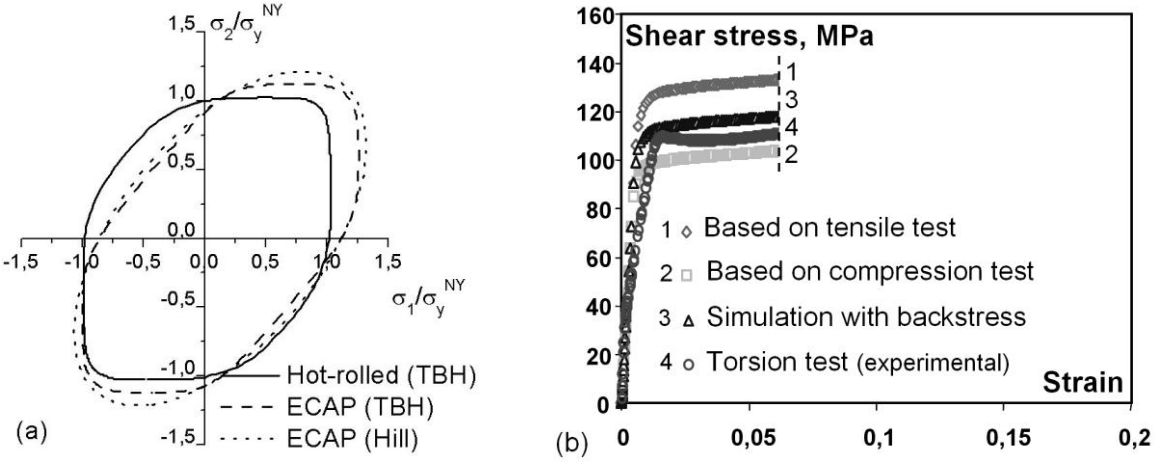

Figure 2 – (a) The initial yield locus shape determined by Hill and TBH. (b) Predicting the torsion results on ECAP material with TBH model, curve 1 and 2 without backstress and with size of yield locus determined by σ_y^t, - σ_y^c and curve 3 with backstress and the size defined by σ_y^{NY}. The apparent hardening comes from simulated compression tests.

This approach to determine the initial yield locus shape and size allows predicting the initial plastic value for all deformation modes, regardless of the strain hardening behavior.

Determining the strain hardening (for ECAP material in compression) – When plasticity is controlled by the dislocation mode, the relation between flow stress and dislocation density ρ can in a first approximation be expressed as $\sigma_Y = M_T \alpha G b \sqrt{\rho}$, where M_T(=3.065) is the tensile Taylor factor here accounting for a random oriented polycrystal, α is a numerical factor (~0.25) depending on the character of the dislocation considered, G is the shear modulus (26GPa for Al) and b is the Burgers vector (b=0.286nm). σ_Y defines the flow stress at a given dislocation density. As a result a rough estimate of the dislocation density can be made. For the tensile test ρ starts from 1.1 10^{15} /m² while for the compression test ρ ~6.4 10^{14}/m² can be estimated. This is a difference of 40% while the initial structures are the same. This is due to the masking effect of internal stresses and indicates that the classical approach will not be accurate enough to represent the real deformation mechanism, although it can still be used as a first approximation. An actual mean initial dislocation density of 8,5 10^{14}/m² could be proposed. The evolution equation of the total dislocation density is formulated by:

$$\frac{d\rho}{d\varepsilon} = M_T \left(k_1 \sqrt{\rho} - k_2 \rho \right) \tag{4}$$

Where k_1 and k_2 are respectively the dislocation generation and annihilation constants. The integration of equation 4 is represented in equation 5, providing an isotropic hardening law.

$$\sigma_F - \sigma_{0.2\%} = Q_h \left(1 - \exp\left(-b_h \left(\varepsilon - \varepsilon_{0.2\%} \right) \right) \right) \tag{5}$$

Where $Q_h = \chi \left(k_1 / k_2 \right)$, $b_h = k_2 \left(M_T / 2 \right)$, $\chi = M_T \alpha G b$

From the macroscopic experimental results, it is possible to estimate the constants from the hardening part of the tensile test (b_h=340, Q_h=14MPa), and from the compression test (b_h=170, Q_h=20MPa). The highest annihilation constant was observed during the tensile test, i.e. more than 2 times the annihilation constant of the compression test. It is important to remark that this approach can not be applied to the apparent softening during tensile testing, as diffuse necking occurs, masking the real stress-strain curve. In torsion it is also not possible to directly apply equation 5 as it is necessary to further investigate the Lüderslike behavior.

Performing FE simulations on the compression sample – The axis of the compression sample was aligned with ED. In fig 3 both the undeformed and 80% deformed sample shapes

are shown. The latter is presented in fig 3(b), the thick lines corresponds to the actual cutting of the sample. The outer lines correspond to the (possible) sample edges. The middle line corresponds to the position of the midplane. FE simulations by Lagamine code are used to compare the final predicted and experimental sample shapes after compression tests. Two yield loci, coupled with the isotropic Voce model (eq. 5) and with the backstress already identified above, have been applied to these simulations: Hill 1948 and the Minty micro-macro model [12] which locally interpolates the stress-strain relation from yield locus points computed by a polycrystal Taylor model based on initial texture description.

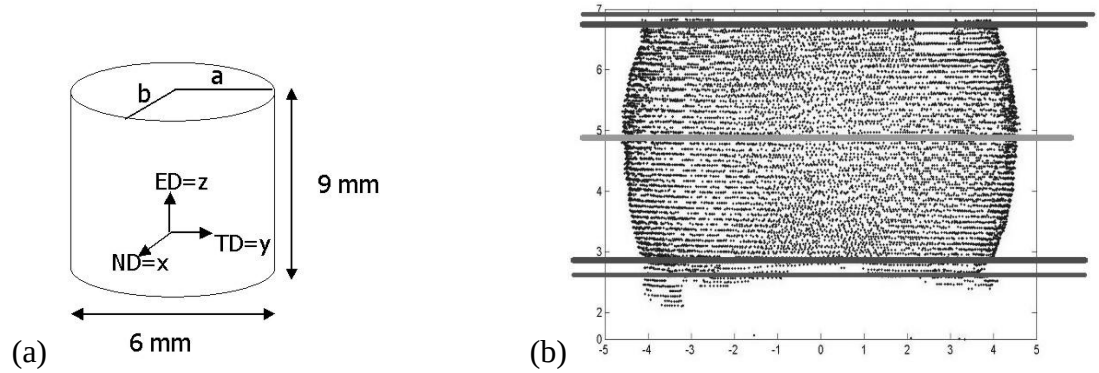

Figure 3 – (a) The original compression sample geometry. (b) Profile measurement on 80% deformed compression sample.

A coefficient of friction equal to 0.1 was used as it minimized the difference between the experimental and numerical data (fig 4). The predicted curves were compared to a 40% and 80% compressive reduction. The profile of geometry is shown for the cylindrical specimen in X-Z and Y-Z sections, as predicted by Hill and Minty coupled with the Voce hardening model. The Minty model shows very close agreement with the experimental results at different stages of deformation. For the Hill model, the computed and experimental results are almost coincident at 40 % reduction, while some deviations can be found at the larger reductions.

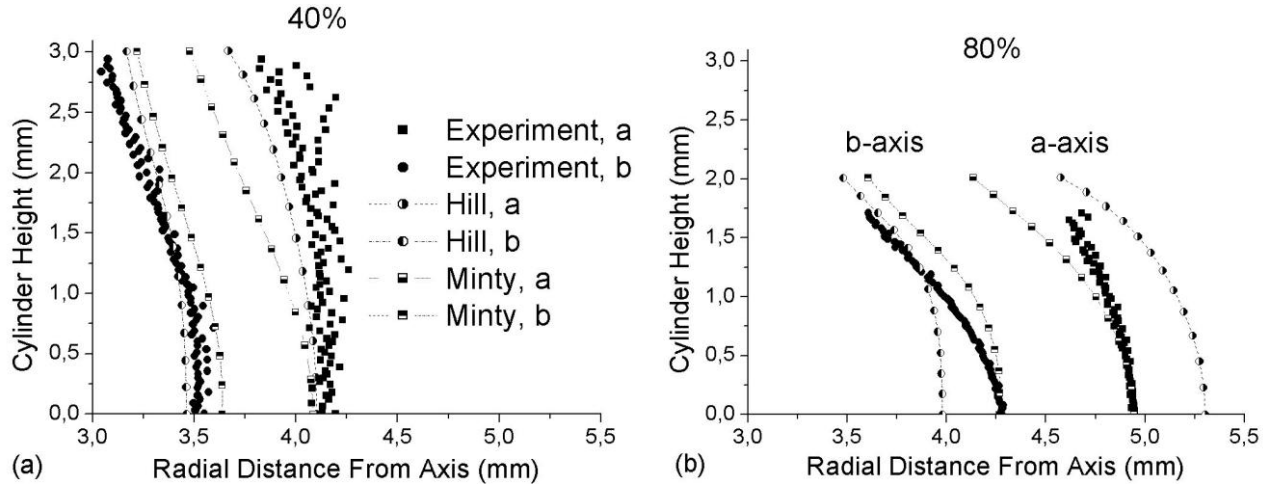

Figure 4 – Profile measurement and simulation on (a) 40% and (b) 80% reduction.

It was postulated that a texture would be of primary importance to strain distribution along the gauge length of the experimental specimen. Hill's model, roughly describing the yield locus, is unable to correctly predict the final shape of the sample. The Minty model provides a closer agreement even not taking into account texture updating during the test. The experimental sample will deform differently depending whether the initial texture of hot-rolled aluminum or the shear texture obtained after ECAP process is present. The predicted shape is compared to experimental observations in fig 5 where the midplane section is shown for both the 40% and 80% reduced samples. The large degree of ellipticity implies that the plastic flow in the cross-section along the midplane for ECAP material is strongly anisotropic, while for an isoptropic material this cross-section would remain circular. It is postulated that the shear texture obtained after ECAP process is responsible for the deviation, which is in agreement with the prediction

from the Minty model based on the texture.

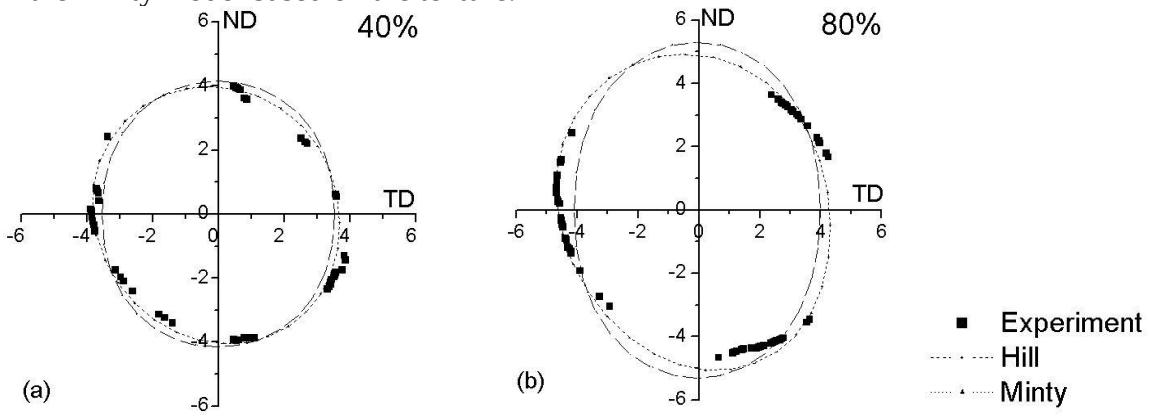

Figure 5 – Midplane measurement and simulation on 40% (a) and 80% (b) reduction.

Summary and Conclusions

ECAP gives an increase in flow stress, and a decrease in ductility. This ductility was mainly restored by an annealing treatment. Comparing compression and tension yield stress, the presence of internal stresses (introduced in the model as a backstress) was demonstrated. This backstress was 21MPa in ECAP material, 8,5MPa in the annealed material and absent in the hot rolled material.

During plastic deformation, the behavior of the three materials is not identical. ECAP material shows no further hardening because during the process the work hardening rate has dropped to zero. After an annealing treatment without causing abnormal grain growth, work hardening is restored. When looking at the different strain hardening stages (torsion test), it can be seen how the hot-rolled material reaches stage III, while both ECAP and annealed ECAP material are able to achieve stage IV.

Simulations on the initial yield locus for the ECAP material showed that an anisotropic Hill function with a proper initial back stress is able to recover the initial flow stress in tension, compression and torsion. A Voce type law was used to model the strain hardening of ECAP material under compression. FE predictions of the shape of the equatorial section of a compressed sample were performed, concluding that the Minty model, coupled with a Voce-type hardening model gave the best agreement with experimental results. For tension and torsion tests, further investigations are needed in order to compensate for inhomogenous deformation and obtain the real stress-strain curve during tension and understand the Lüderslike straining for the torsion test.

Acknowledgement

This study was carried out in the frame of project IAP, P5/08 financed by Belgian Science Policy. The authors also acknowledge the funding provided by the FWO project G.0208.02. A.M. Habraken is mandated by the National Fund for Scientific Research (Belgium).

References

1. Conrad H., Narayan J., Acta Materialia, Vol. 50 (2002), 5067-5078
2. Humphreys F.J., Prangnell P.B., Bowen J.R., Gholinia A. and Harris C., Phil. Trans. R. Soc. London Vol.A357 (1999), 1663-1681
3. Poortmans S., Verlinden B., Materials Science Forum, Vols. 467-470 (2004), 1319-1324
4. Poortmans S., Verlinden B., Mat. Science Forum , Vols 503-504, (2006), 847-852
5. Dupuy L., Rauch E.F., Mat. Sci. Eng., Vol. A 337(2002), 241-247
6. Chinh N.Q., Vörös G., Horita Z., Langdon T.G., Proceedings of Ultrafine Grained Materials II, TMS, Washington (2002), 567-574
7. Turner T.J., Miller M.P., Barton N.R., Mechanics of Materials, Issue 34 (2002), 605-625
8. De Messemaeker J., Verlinden B., Van Humbeeck J., Mat. Lett., Vol. 58 (2004), 3782-3786
9. Dieter G.E., Mechanical Metallurgy, McGraw-Hill, London, 1988
10. May J., Höppel H.W., Göken M., Scripta Materialia, Vol 53 (2005), 189-194
11. Hart E.W., Acta Metallurgica, Vol. 15 (1967), 351-355
12. Habraken A.M., Duchêne L., Int. Journal of Plasticity, Vol 20, Issue 8-9 (2004), 1525-1560